DOI:
10.1161/CIRCIMAGING.117.007453

Document Version
Publisher's PDF, also known as Version of record

Circulation: Cardiovascular Imaging

ORIGINAL ARTICLE

Simultaneous Assessment of Cardiac Inflammation and Extracellular Matrix Remodeling After Myocardial Infarction

See Editorial by Lanza

Isabel T. Ramos, PhD
Markus Henningsson, PhD
Maryam Nezafat, PhD
Begoña Lavin, PhD
Silvia Lorrio, PhD
Pierre Gebhardt, PhD
Andrea Protti, PhD
Thomas R. Eykyn, PhD
Marcelo E. Andia, MD, PhD
Ulrich Flögel, PhD
Alkystis Phinikaridou, PhD
Ajay M. Shah, MD, FMedSci
René M. Botnar, PhD

BACKGROUND: Optimal healing of the myocardium after myocardial infarction (MI) requires a suitable degree of inflammation and its timely resolution, together with a well-orchestrated deposition and degradation of ECM (extracellular matrix) proteins.

METHODS AND RESULTS: MI and SHAM-operated animals were imaged at 3, 7, 14, and 21 days with 3T magnetic resonance imaging using a $^{19}F/^{1}H$ surface coil. Mice were injected with ^{19}F-perfluorocarbon nanoparticles to study inflammatory cell recruitment, and with a gadolinium-based elastin-binding contrast agent to evaluate elastin content. ^{19}F magnetic resonance imaging signal colocalized with infarction areas, as confirmed by late gadolinium enhancement, and was highest 7 days post-MI, correlating with macrophage content (MAC-3 immunohistochemistry; ρ=0.89, P<0.0001). ^{19}F quantification with in vivo (magnetic resonance imaging) and ex vivo nuclear magnetic resonance spectroscopy correlated linearly (ρ=0.58, P=0.020). T_1 mapping after gadolinium-based elastin-binding contrast agent injection showed increased relaxation rate (R_1) in the infarcted regions and was significantly higher at 21 days compared with 7 days post-MI (R_1 [s^{-1}]: 21 days=2.8 [interquartile range, 2.69–3.30] versus 7 days=2.3 [interquartile range, 2.12–2.5], P<0.05), which agreed with an increased tropoelastin content (ρ=0.89, P<0.0001). The predictive value of each contrast agent for beneficial remodeling was evaluated in a longitudinal proof-of-principle study. Neither R_1 nor ^{19}F at day 7 were significant predictors for beneficial remodeling (P=0.68; P=0.062). However, the combination of both measurements (R_1<2.34 Hz and 0.55≤^{19}F≤1.85) resulted in an odds ratio of 30.0 (CI 95%, 1.41–638.15; P=0.029) for favorable post-MI remodeling.

CONCLUSIONS: Multinuclear $^{1}H/^{19}F$ magnetic resonance imaging allows the simultaneous assessment of inflammation and elastin remodeling in a murine MI model. The interplay of these biological processes affects cardiac outcome and may have potential for improved diagnosis and personalized treatment.

Key Words: extracellular matrix ■ macrophage ■ magnetic resonance imaging ■ molecular imaging ■ myocardial infarction

https://www.ahajournals.org/journal/circimaging

CLINICAL PERSPECTIVE

Here, we developed a new multinuclear magnetic resonance imaging protocol that allows visualizing and quantifying myocardial inflammation and ECM (extracellular matrix) remodeling simultaneously in a murine model of permanent coronary occlusion. The imaging approach is based on $^{19}F/^{1}H$ multinuclear magnetic resonance imaging in concert with fluorine nanoparticles and a gadolinium-based elastin-specific magnetic resonance contrast agent. This is the first study that assessed inflammation and ECM remodeling simultaneously with a single noninvasive imaging modality and could provide important insights in post-infarct remodeling in patients developing heart failure. We also demonstrated the prognostic value of quantifying inflammation and ECM remodeling 7 days post-MI. A well-balanced inflammatory response was beneficial for maintaining left ventricular function, whereas extensive ECM remodeling was detrimental. If translated into the clinic, this work could provide clinicians with a new tool to noninvasively assess inflammation and ECM remodeling (focal and diffuse fibrosis), which is not possible with currently available contrast agents or noncontrast enhanced imaging methods. In summary, we demonstrated the feasibility of measuring myocardial inflammation and ECM remodeling (fibrosis) noninvasively, 2 key processes in tissue injury, and has great potential beyond cardiac imaging such as for the assessment of renal, liver or lung inflammation, and fibrosis.

Cardiac injury activates innate immunity, which initiates an inflammatory response whereby neutrophils and monocytes/macrophages are recruited to the myocardium.[1] Immediately after myocardial infarction (MI), neutrophils are recruited to the site of injury, followed by the recruitment of monocytes/macrophages that remove dead cells and debris by phagocytosis.[1,2] Studies have shown that an early and aggressive immune response and high levels of neutrophils and monocytes within the infarct may promote adverse remodeling and lead to poor prognosis.[3,4] In addition to their phagocytic properties, inflammatory cells activate reparative pathways, including the formation and deposition of scar tissue, which is mainly composed of collagen and elastin/tropoelastin.[2,5,6] Elastin has been shown to be essential for the stabilization of the scar after MI and improving cardiac function by preserving elasticity.[7,8] While the healthy myocardium contains elastin only to a negligible degree within the interstitium and coronary vasculature, an increase of elastic fibers within the myocardial scar is detected in the first weeks after ischemic injury developing a dense network between the remaining viable myocytes, myofibroblasts, and smooth muscle cells during the maturation of the infarct.[5] Tropoelastin, the soluble precursor of elastin, is synthesized in significant amounts and deposited within the remodeled myocardium, particularly at later stages of the healing process.[9]

Magnetic resonance imaging (MRI) has great potential to noninvasively assess both structure and function of the heart. By combining MRI with specific contrast agents, different biological processes can be targeted and tracked over time. In this study, we sought to explore the merits of multinuclear $^{1}H/^{19}F$ MRI for the sequential assessment and quantification of cardiac inflammation and elastin remodeling in a murine model of MI using a 3T clinical scanner. Perfluorocarbons (PFCs) were used to assess inflammatory cell recruitment and gadolinium-based elastin-specific magnetic resonance contrast agent (Gd-ESMA) was used for the investigation of elastin deposition and quantification of ECM (extracellular matrix) remodeling of the myocardium. This approach may potentially allow a more accurate characterization of early or persistent inflammation and diffuse myocardial remodeling at the molecular level. It may also serve as a new biomarker for monitoring treatment response and evaluation of novel cardioprotective therapies.

METHODS

The DICOM MR images will be made available to other researchers for purposes of reproducing the results.[10]

Animal Model

The institutional subcommittee on research animal care approved all animal studies. MI was induced in 10-week-old female C57BL/6J mice (n=71; 21% mortality rate; Charles River, United Kingdom) by permanent occlusion of the left anterior descending (LAD) coronary artery. Mice were anesthetized by intraperitoneal injection of 75 mg/kg ketamine (Vetalar V, Vetmedica) and 1 mg/kg medetomidine hydrochloride (Domitor, Orion Corporation, Finland). The animals underwent endotracheal intubation before surgery using an animal ventilator (Hugo Sacks Elektronic, Germany). A left thoracotomy was performed in the fourth intercostal space, the pericardium removed, and the LAD was permanently ligated with an 8-0 nylon suture (Direct Medical Supplies, Alton, United Kingdom). Successful ligation was confirmed by the regional blanching of the left ventricle (LV), extending to the apex. After thoracotomy, subcutaneous tissue and skin were closed in separate layers and the animal was weaned from the ventilator. After the surgery, mice were monitored and maintained in a heated chamber for at least 6 hours. Sham-operated animals underwent the same surgical procedure, without LAD ligation. Thirty minutes before recovery, 0.15 mg/kg buprenorphine (Vetergesic, Alstoe, United Kingdom) was administered for analgesia by intramuscular injection.

Magnetic Resonance Imaging

In vivo cardiac scans were performed using a 3T Philips Achieva MR scanner (Philips Healthcare, Best, The Netherlands) equipped with a clinical gradient system (30 mT/m, 200 mT/m per ms). Mice (n=8 per time-point) were imaged at 3, 7, 14, and 21 days post-MI. Sham-operated mice (n=6 per time-point) were imaged at the same time-points and were used as controls (Figure 1A). Fifteen mice were imaged longitudinally at 7 and 21 days post-MI (Figure 1B). Animals were placed in a prone position on a $^{19}F/^{1}H$ surface coil (Rapid Biomedical, Würzburg, Germany; diameter=23 and 33 mm). Anesthesia was induced with 5% and maintained with 1.5% to 2% isoflurane in medical oxygen during the MRI scan, and the body temperature was measured with a rectal temperature probe and maintained at 35±1°C using a water-based heating system (SA Instruments, Stony Brook, NY). ECG was monitored with 2 metallic needles placed subcutaneously in the region of the chest. ^{1}H and ^{19}F cardiac ECG-triggered MR images were acquired 48 hours after intravenous injection of 400 µL of 10% perfluoro-15-crown-5 ether emulsion (PFC), as previously described[11] and 0.5 mmol/kg of a gadolinium-based MRI contrast agent that targets elastin and tropoelastin, Gd-ESMA (Lantheus Medical Imaging, North Billerica, MA), administered 1 hour before the MRI scan. At the end of the scans, the mice were culled and the heart was extracted for histological and nuclear magnetic resonance (NMR) studies.

After a 3-dimensional (3D) gradient echo scout scan, 2D cine short-axis images, covering the entire LV, were acquired to analyze functional and volumetric parameters. Imaging parameters were field-of-view (FOV)=35×35×12 mm^3, acquired in-plane resolution=0.3×0.3×1 mm^3, slices=12, repetition time (TR)/echo time=7.8/16.0 ms, flip angle=20°. Subsequently, a 2D Look-Locker scan planned perpendicular to the LV was used to determine the optimal inversion time for nulling of the healthy myocardium. Three-dimensional short-axis late gadolinium enhancement (LGE) gradient echo images were acquired between 60 and 80 minutes after Gd-ESMA injection for the visualization of contrast uptake within the infarcted region with the following parameters: FOV=35×35×12 mm^3, acquired in-plane resolution=0.3×0.3×1 mm^3, slices=12, TR/TE=6.4/2.6 ms, 5 heartbeats between subsequent inversion recovery pulses, and flip angle=25°. T_1 mapping was performed using a 2D Modified Look-Locker inversion recovery sequence.[12] The inversion pulse was followed by 8 segmented readouts, each spaced 1 R-R intervals in cardiac gating apart, for 8 individual images resulting in inversion time's ranging from 10 to 2000 ms. To allow full magnetization recovery, 12 pauses/heartbeats were performed before the next inversion pulse. Acquisition parameters included FOV=35×35×1.5 mm^3, acquired in-plane resolution=0.3×0.3 mm^2, slices=1, TR/TE=7.5/3.1 ms, flip angle=16 °. For the visualization of the inflammatory cells, a 3D turbo spin echo ^{19}F scan was acquired with a FOV=35×35×12 mm^3, acquired in plane resolution=1×1×2 mm^3, slices=12, TR/TE=4 beats/8.9 ms, turbo spin echo factor=5, offset frequency=10 200 Hz (BW=6103 Hz). A saturation slice was used to suppress the liver signal. To enable signal-to-noise (SNR) calculation, a noise scan was acquired with the same imaging parameters but without any radiofrequency pulses to correct for local noise variability. A T_2-weighted sequence was used to analyze edema within the heart at 3 and 7 days post-MI, with the following parameters: FOV=35×35×1.5 mm^3, acquired in-plane resolution=0.3×0.3 mm^2, slices=3, TR/TE=126/18 ms, flip angle=30°.

MR Image Analysis

Ejection fraction (%), LV end-diastolic volume (LVEDV, µL) and LV mass (mg) were calculated from the cine images, using an automated segmentation software (ClinicalVolumes, King's College London, www.clinicalvolumes.com).[13] Total infarct size was calculated by adding the LGE measured on consecutive slices after the administration of Gd-ESMA (LGE-ESMA). The sum of the total infarcted area was multiplied by the slice thickness to generate a volume (mm^3) and was then divided by the total LV myocardium and expressed as percentage. T_1 relaxation times (R_1) were calculated by manually segmenting T_1 map regions corresponding to the LGE-ESMA using OsiriX (Osirix Foundation, Geneva, Switzerland). For ^{19}F measurements, regions of interest were defined as areas of enhancement seen on the LGE-ESMA images. For these areas, 19F

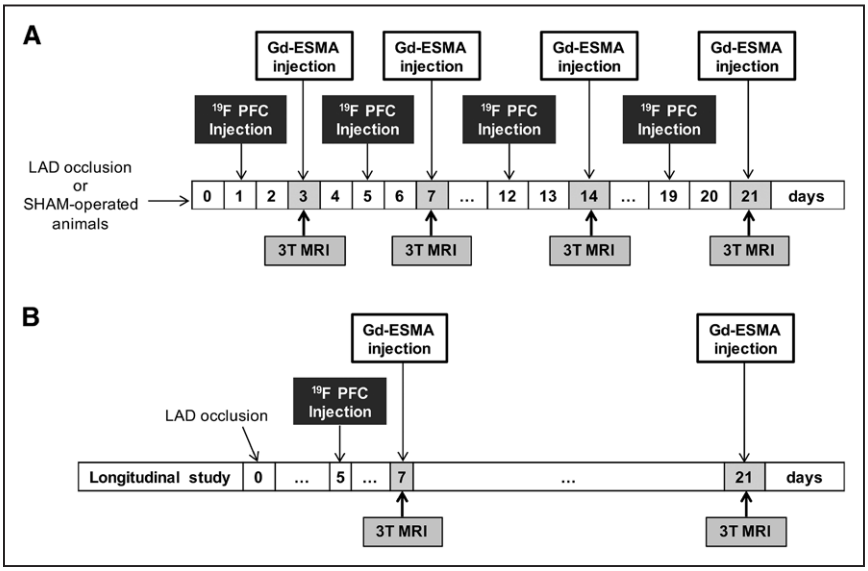

Figure 1. Experimental study design. Myocardial infarction was induced in C57Bl6 female mice after permanent occlusion of the left anterior descending (LAD) coronary artery. Magnetic resonance imaging (MRI) scans were performed after intravenous injection of ^{19}F perfluorocarbons (^{19}F PFCs) and gadolinium-based elastin/tropoelastin specific MR contrast agent (Gd-ESMA), 48 and 1 h before imaging sessions, respectively. **A**, Mice (n=8 per group/time-point) were imaged at 3, 7, 14, and 21 days post-myocardial infarction (MI). SHAM-operated mice (n=6 per group/time-point) were imaged at the same time-points and were used as controls. At the end of the scans, mice were culled and hearts were extracted for histology and nuclear magnetic resonance (NMR; n=4/group and 3-SHAM-operated animals/time-point for each technique). **B**, 15 mice were imaged longitudinally at 7 and 21 days post-MI.

signal was calculated using the following equation: $^{19}\text{F signal} = \frac{\sum \text{SNR}}{\text{scar volume}}$, where SNR is the sum of the signal of the infarcted area divided by the SD of the noise in each slice, and scar volume was calculated from the sum of the LGE-ESMA area of each slice multiplied by the MRI slice thickness.[14]

Nuclear Magnetic Resonance Spectroscopy

NMR spectroscopy was used to quantify the uptake of PFC ex vivo. Mice injected with PFC and scanned at 3T were culled and the hearts were collected (MI, n=4; SHAM, n=3; each per time-point). Remote and infarcted regions were separated, weighed and frozen at –20ºC before NMR analysis. NMR spectra of the PFCs were recorded at room temperature using a Bruker Avance III 9.4T scanner (^{1}H 400 MHz; ^{19}F 375.8 MHz) and a 15-mm-diameter-large, double-tuned (^{31}P/^{1}H) volumetric microimaging coil. The water resonance was used to shim the sample and the ^{1}H coil was then retuned to the ^{19}F frequency. Both remote and infarcted areas were placed in NMR tubes (Fisher Scientific, Leicestershire, United Kingdom) with a silicone support to position the sample within the isocentre of the coil. A sealed external reference capillary of 100% trifluoroacetic acid (TFA) solution (δ-TFA=–76.6 ppm as identified in the literature, and reported relative to $CFCl_3$) was placed adjacent to the heart. The ^{19}F NMR chemical shift of the PFC peak was –12.5 ppm relative to the reference capillary. A 90º radiofrequency pulse (30 μs hard pulse) was used together with many signal averages=64, total experiment duration=4.78 min, time domain size=131 K data points, prescan delay=1 second, acquisition time=3.5 seconds to give a total repetition time of TR=4.5 seconds per scan, spectral bandwidth=18 797 Hz. Data were processed with an exponential line broadening factor (20 Hz), followed by Fourier transformation, zero- and first-order phase correction and automatic baseline correction. Peaks corresponding to the TFA reference and the PFC were integrated using Topspin 2.1 software (Bruker Biospin GmbH, Rheinstetten, Germany) and normalized to the reference capillary. The number of moles of ^{19}F was calculated using the equation $[\text{PFC}] = \frac{N_{TFA} \times I_{PFC} \times [\text{TFA}]}{N_{PFC} \times I_{TFA} \times g_{tissue}}$, where [PFC] is the concentration per gram tissue (wet weight), N_{TFA} is the number of ^{19}F nuclei giving rise to the TFA signal, N_{PFC} is the number of ^{19}F nuclei giving rise to the PFC signal, I_{PFC} is the peak integral of the PFC peak, I_{TFA} is the peak integral of the TFA peak (I_{TFA}=1, normalized), [TFA] is the number of moles of TFA.

Histology

After the MRI scans, anesthetized mice were culled by neck dislocation and hearts were collected for ex vivo analysis (n=4 MI mice per time-point, and n=3 SHAM-operated animals per time-point). Hearts were harvested, the atriums were removed and the ventricles were washed in saline solution followed by immersion in 10% formaldehyde solution for 24 hours at room temperature. Hearts were then dehydrated, paraffin-embedded, and transversely sectioned (5 μm thick).

Immunohistochemistry (IHC) was used to quantify the amount of tropoelastin and macrophages in the myocardium. Tropoelastin was detected with anti-mouse rabbit polyclonal antibody (21600, Abcam; dilution 1:100) using an avidin-biotin-peroxidase method (Vector SG Peroxidase substrate; Vector Laboratories, Burlingame, CA). A monoclonal rat anti-mouse antibody (550292, BD Pharmingen; CD107b; MAC-3; dilution 1:100) was used for macrophage detection. The antibody was revealed with streptavidin-peroxidase (Dako, Ely, United Kingdom; ABC kit, 1:100). Digital images were analyzed using ImageJ (National Institute of Health, Bethesda, MD). Tropoelastin and MAC-3 were quantified and expressed as percentage of the infarcted myocardium using ImageJ, and were manually segmented and normalized with the total area of infarction for each histology slice calculated from Masson's trichrome staining.

Statistical Analysis

GraphPad Prism 5.00 (GraphPad Software, Inc, La Jolla, CA) was used for statistical analysis. Nonparametric exact tests were used for analysis. Differences between different time-point measurements were analyzed using Kruskal-Wallis test for multiple group comparisons, and if this test was significant, it was followed by Dunn's post hoc test. Differences between different time-points and different groups: SHAM/scar/remote were analyzed using a 2-way ANOVA. Correlations were assessed using Spearman rank test. To study the nonlinear behavior of ^{19}F in the longitudinal study, the linear correlation model was compared with second-order polynomial model regression; both variables (EDV at day 21 and ^{19}F SNR) were first tested for normal distribution using the D'Agostino-Pearson omnibus normality test. Receiver operating characteristic curve analysis was performed to identify the cutoff point of imaging biomarkers to predict the evolution of functional cardiac parameters; in this case, the increase in the LVEDV between day 7 and day 21 was considered as dysfunctional remodeling, and the decrease of EDV between day 7 and day 21 was considered as a beneficial remodeling. $P<0.05$ was considered statistically significant. Data are presented as median, and interquartile range (IQR).

RESULTS

Assessment of Cardiac Function by MRI at 3T

Cardiac function was assessed using cine MRI and results are summarized in Figure 2 (detailed results in Table I in the Data Supplement). A visual enlargement of the LV and thinning of the ventricular wall at the site of the infarction was observed post-MI and became more evident at day 21. These results are consistent with previous studies in the same animal model.[15]

Assessment of the Inflammatory Response in Post-MI Remodeling Using PFCs

Myocardial remodeling post-MI is associated with an acute inflammatory response. Combined proton (^{1}H) and fluorine (^{19}F) images confirmed colocalization of the PFCs within the infarcted area at both 3 and 7 days (Figure 3A).

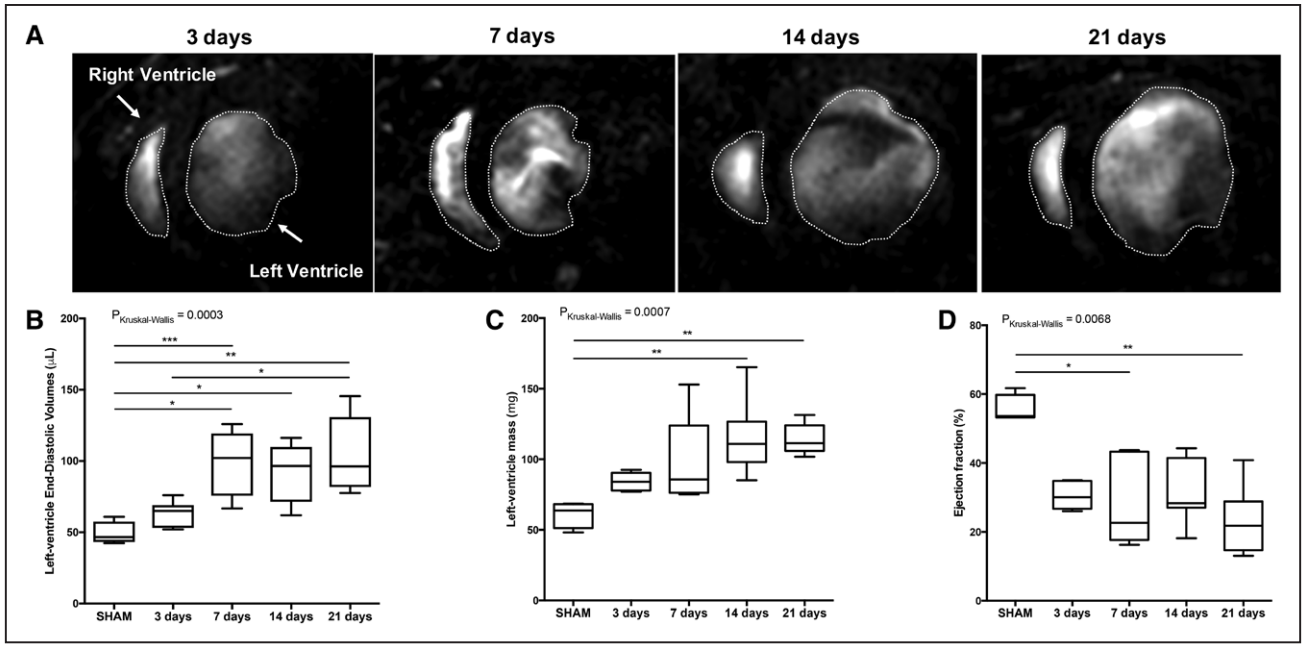

Figure 2. Functional and volumetric parameters of the heart at 3, 7, 14, and 21 days post-myocardial infarction (MI) and SHAM-operated mice. **A**, Representative anatomic short-axis images of the heart. Myocardium is depicted in orange; the star indicates myocardial wall thinning at day 21. **B**, Left ventricular end-diastolic volume progressively dilates from acute to late stages of MI. **C**, Increasing Left ventricular mass and (**D**) decreasing ejection fraction were observed over time. N=8 MI animals/time-point, N=4 SHAM-operated animals/time-point. *P<0.05, **P<0.01.

Quantitative in vivo ^{19}F MRI showed a significant increase of ^{19}F signal (SNR/scar volume) within the infarcted area at 7 days post-MI (SNR=1.27 [IQR, 0.84–1.58]) compared with SHAM-operated animals (SNR=0.19 [IQR, 0.13–0.20]; P<0.001) (Figure 3B). A maximum ^{19}F signal was observed at 7 days post-MI which was significantly greater than at 3 days (SNR=0.44 [IQR, 0.39–0.67]; P<0.05), 14 days (SNR=0.30 [IQR, 0.23–0.34]; P<0.01). At 21 days post-MI (SNR=0.18 [IQR, 0.15–0.28] the ^{19}F signal was negligible and significantly lower compared with 3 days (P<0.05) and 7 days (P<0.001), consistent with the resolution of inflammation. ^{19}F signal was also detected at the site of thoracotomy, in the liver and lymph nodes, as these are major sites of macrophage clearance. Although the spleen was outside our imaging volume, PFC uptake would be also expected in this organ (as seen by other studies).[16]

To verify the in vivo results and to quantify the evolution of the ^{19}F signal, infarcted and remote areas were dissected and separated for ex vivo NMR spectroscopy acquired on whole tissue samples. NMR spectra were in good agreement with the in vivo MRI findings, where infarcted regions showed high PFC signal that was absent in the remote myocardium (Figure 3C). NMR analysis showed a maximum ^{19}F concentration (mmol/g tissue) at 7 days post-MI ([^{19}F]=0.12 [IQR, 0.075–0.18]; P<0.05) that was significantly higher compared with 21 days post-MI ([^{19}F]=0.0063 [IQR, 0.0042–0.020]). At 7 days post-MI the uptake in the region of infarcted myocardium was significantly greater than both remote myocardium ([^{19}F]=0.026 [IQR, 0.015–0.057]; P<0.05) and healthy hearts from SHAM-operated animals ([^{19}F]=0.012 [IQR, 0.0042–0.044]; P<0.05). At 21 days post-MI, the signal in the remote myocardium was statistically different from SHAM-operated animals. In SHAM-operated animals injected with PFC, no ^{19}F signal was detected in the heart. A linear correlation was observed between in vivo MRI measurements and ex vivo NMR ^{19}F signal measurements (ρ=0.58; P=0.020; Figure I in the Data Supplement).

MAC-3 IHC for identification of myocardial tissue macrophages showed recruitment of these cells into the infarcted area at the early stages after MI but not to the remote myocardium as seen by in vivo imaging (Figure 3A). The number of MAC-3 positive macrophages was significantly higher at 3 days post-MI (IHC_{MAC-3}[%]=2.12 [IQR, 1.88–2.63]; P<0.05) and 7 days post-MI (IHC_{MAC-3}[%]=3.65 [IQR, 2.74–4.09]; P<0.01) compared with SHAM animals (IHC_{MAC-3}[%]=0.003 [IQR, 0.002–0.004]) and was significantly higher at 7 days post-MI compared with 21 days post-MI (IHC_{MAC-3}[%]=0.13 [IQR, 0.041–0.23]; P<0.05; Figure 3D). There was a significant correlation between the in vivo ^{19}F MRI signal and macrophage content as quantified by IHC (ρ=0.89; P<0.0001; Figure 3E).

Assessment of Elastin Remodeling Post-MI Using Gd-ESMA

ECM remodeling post-MI was evaluated using Gd-ESMA, a contrast agent that binds to both cross-linked

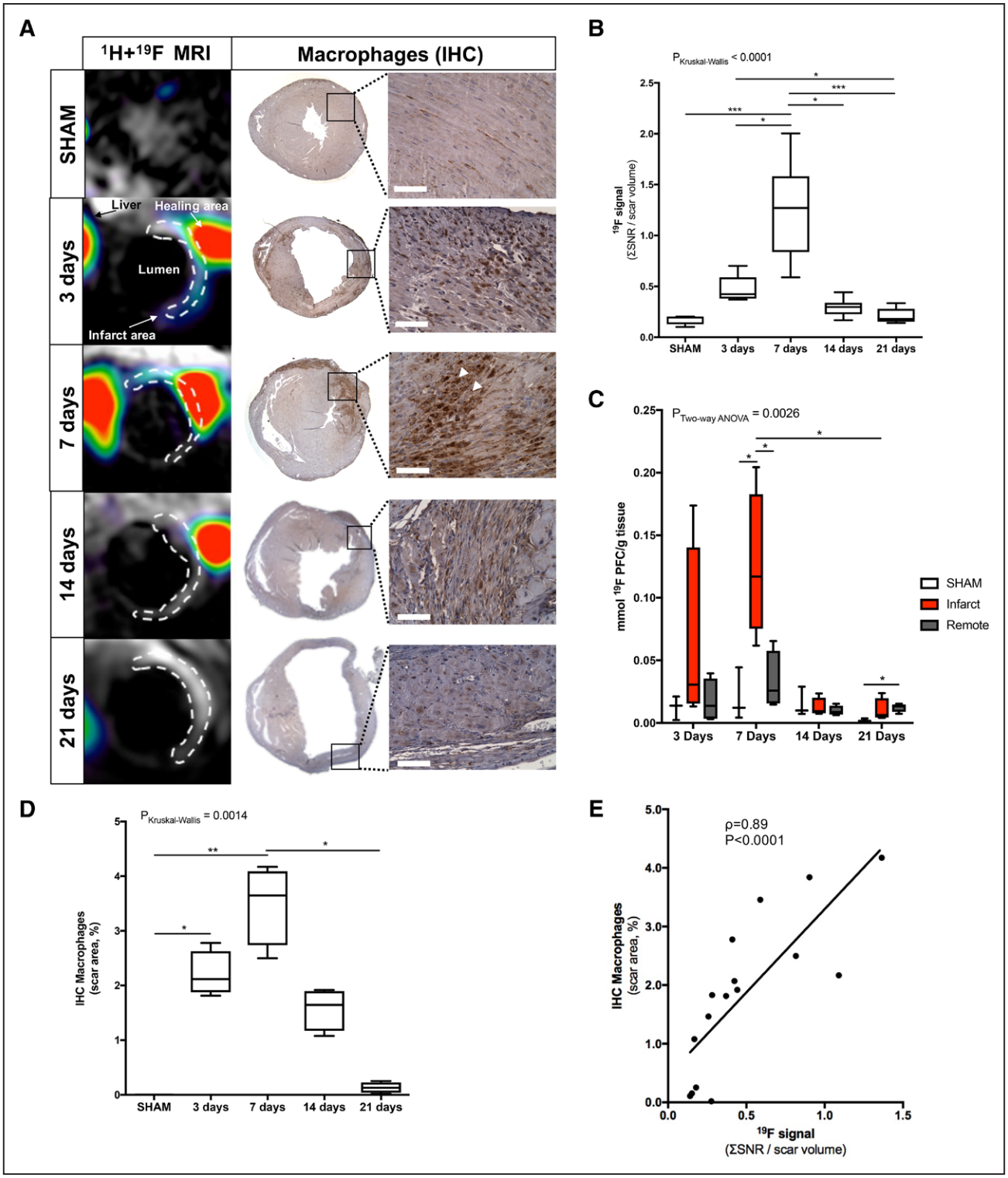

Figure 3. Assessment of inflammatory response after myocardial infarction in mice at 3T magnetic resonance imaging (MRI) using 19F perfluorocarbons.

A, Representative short-axis views of coregistered $^{1}H+^{19}F$ images (left column; N=8 MI animals/time-point; N=6 SHAM-operated animals/time-point) and macrophage immunohistochemistry (IHC; macrophages identified as MAC-3 positive, brown; N=4 MI animals/time-point; N=3 SHAM-operated animals/time-point) from the heart at 3, 7, 14, and 21 days after MI. **B,** In vivo ^{19}F MRI signal quantification. **C**, Ex vivo, ^{19}F nuclear magnetic resonance (NMR) signal quantification (N=4/time-point, N=3 SHAM-operated animals). **D**, IHC macrophages quantification shown a significant decrease between 7 and 21 days after infarct. **E**, Correlation between ex vivo macrophages IHC and in vivo ^{19}F MRI signal. Spearman correlation (N=20, ρ=0.89, $P<0.0001$). Scale bar, 50 μm. $*P<0.05$, $**P<0.01$, $***P<0.001$. IHC indicates immunohistochemistry.

elastin and immature tropoelastin.[17,18] One hour post-Gd-ESMA injection, infarcted areas were enhanced at all time-points post-MI, allowing quantification of infarct size. Trichrome staining was performed and used to quantify infarct size ex vivo. There was a strong linear correlation between infarct size measured by in vivo MRI and histology (ρ=0.85; P<0.0001; Figure II in the Data Supplement).

To understand the contribution of fluid accumulation in the interstitial space to the MR signal early after MI, myocardial edema was assessed using a T_2-weighted sequence.[19–21] The high signal was observed at day 3 but not at day 7 post-MI. The signal intensity seen on T_2-weighted images at day 3 was associated with edema and increased extracellular volume, but did not reflect deposition of elastin/tropoelastin as confirmed by histology (Figure 4).

In vivo quantification of Gd-ESMA uptake was performed using a Modified Look-Locker inversion T_1-mapping sequence. Relaxation rate (R_1) maps showed uptake of Gd-ESMA in the infarcted area (increased R_1) at 3, 7, 14, and 21 days post-MI, whereas no enhancement was observed in the remote myocardium (infarct versus remote, P<0.01, Figure 5B) nor in the SHAM-operated animals (infarct versus SHAM, P<0.001, Figure 5B). R_1 values were also significantly higher within the infarct area at 21 days (R_1 [s^{-1}]=2.83 [IQR, 2.69–3.30]; P<0.05) compared with 7 days (R_1 [s^{-1}]=2.3 [IQR, 2.12–2.5]).

To analyze the deposition of elastin fibers in the heart after MI, Elastica van Gieson staining was performed. Mature fibers could be visualized, however, quantification was challenging (Figure III in the Data Supplement). For that reason, tropoelastin IHC was performed (Figure 5A and 5C) revealing a dense fiber network within the infarcted myocardium at 14 and 21 days post-MI but not in the remote myocardium. Tropoelastin deposition was significantly higher at both 14 days ($IHC_{Tropoelastin}$[%]=2.78 [IQR, 2.51–3.07]) and 21 days ($IHC_{Tropoelastin}$[%]=3.25 [IQR, 2.87–3.45]) compared with SHAM ($IHC_{Tropoelastin}$[%]=0.14 [IQR, 0.13–0.15], P<0.01). For the reason abovementioned, the 3 days' time-point was excluded from the correlation analysis between R_1 and tropoelastin IHC analyses. There was a statistically significant correlation between R_1 values from 7, 14, and 21 days measured in vivo and ex vivo IHC analysis (ρ=0.89; P<0.0001; Figure 5D).

^{19}F Versus R_1 Can Be Used to Predict Cardiac Remodeling: Longitudinal Study

Remodeling post-MI is a dynamic and complex process. To understand the potential prognostic value of in vivo ^{19}F and Gd-ESMA MRI, a longitudinal proof-of-principle study was performed. Fifteen animals were scanned twice at days 7 and 21 post-MI. ^{19}F MRI was performed at 7 days post-MI to assess the peak in the inflammatory response and MRI with Gd-ESMA was performed at days 7 and 21 post-MI. No correlation was found between ^{19}F at day 7 post-MI and Gd-ESMA uptake at day 7 (Figure 6A) and at day 21 post-MI (Figure 6B), suggesting that these biological processes are independent/decoupled from each other.

The presence of elastin at day 7 (measured as R_1) showed a linear correlation with the EDV measured at day 21, suggesting that early accumulation of elastin/tropoelastin (larger Gd-ESMA uptake at day 7) might not be beneficial for the healing of the myocardium at day 21 (Figure 7A). In contrast, the inflammatory process measured at day 7 showed a more complex behavior (second-order polynomial model regression showed significant correlation than the linear model (P=0.030). PFCs data suggest that an optimal inflammatory response was observed for a ^{19}F signal range between 0.55 and 1.85. Both an increased (^{19}F>>1.85) or weak (^{19}F<<0.55) inflammatory response at early stages post-MI resulted in large EDV (EDV>100 µL) at day 21 suggesting adverse cardiac outcome (Figure 7B).

The prognostic value of the ^{19}F signal (^{19}F SNR) and quantitative assessment of elastin/tropoelastin deposition (R_1) was investigated with receiver

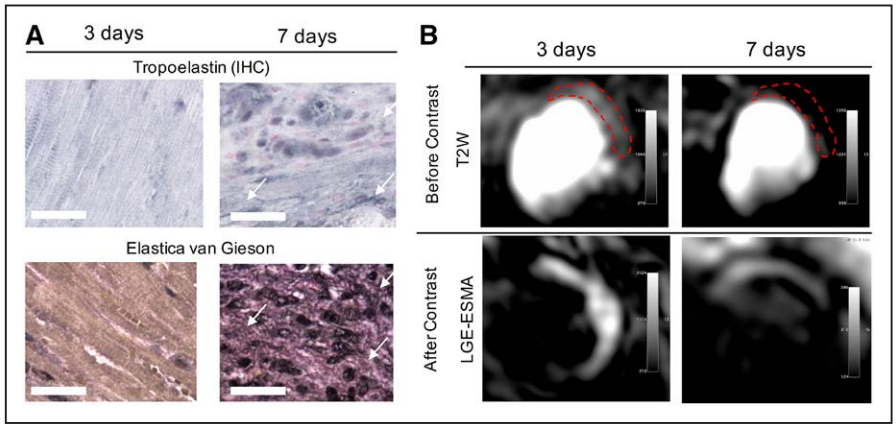

Figure 4. Assessment of elastin/tropoelastin and myocardial edema in mice with myocardial infarction.
A, Tropoelastin immunohistochemistry (IHC) and Elastica van Gieson (black staining) reveal the absence of protein deposition within the heart at 3 days, starting to accumulate at day 7 (arrows). **B**, T_2-weighted images showing high-signal intensity on the lateral wall (top images); Contrast-enhanced image (late gadolinium enhancement) showing high-signal intensity in the infarcted areas (middle images). Scale bar, 25 µm.

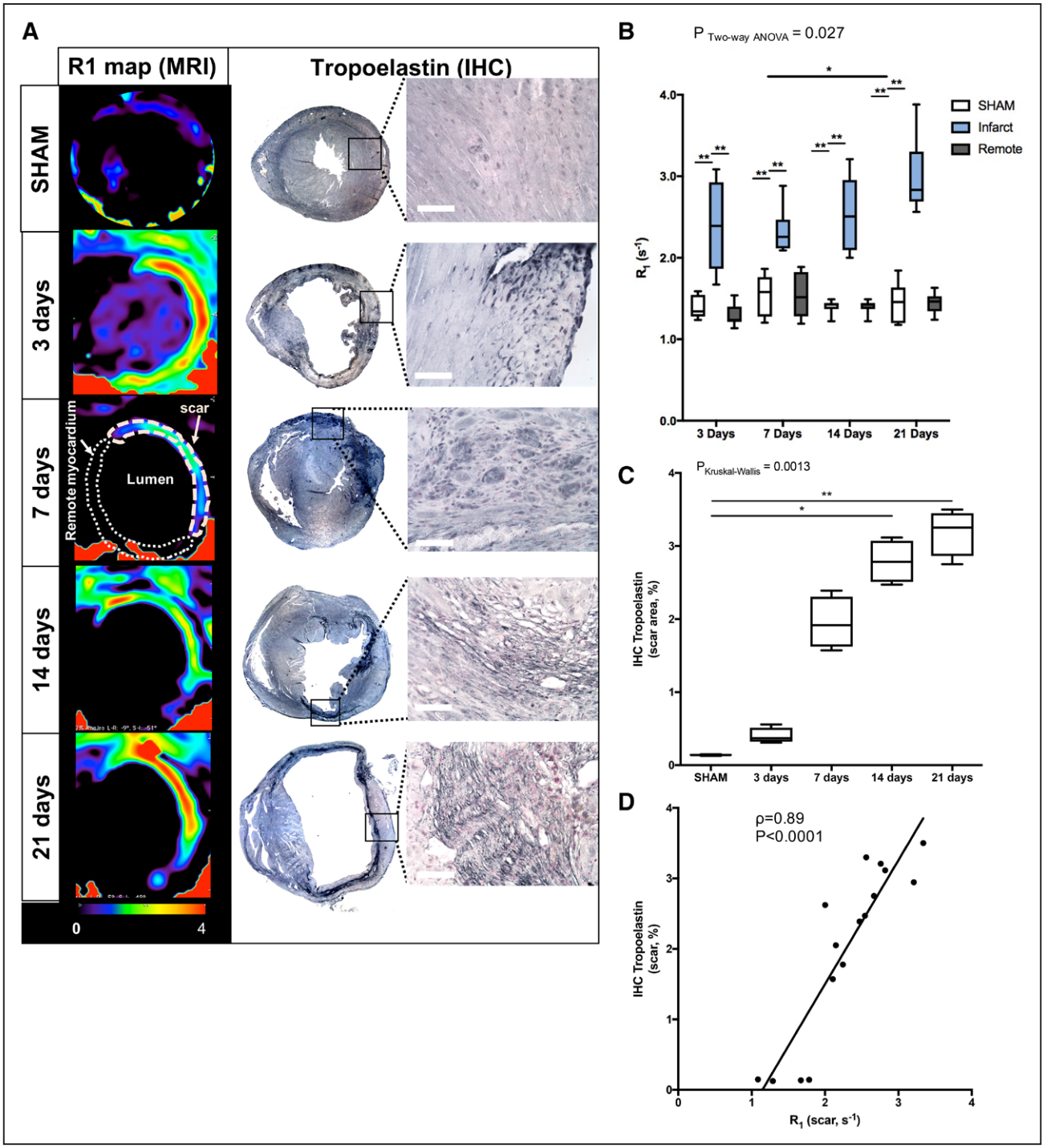

Figure 5. In vivo imaging of extracellular matrix remodeling after myocardial infarction with a gadolinium-based elastin/tropoelastin-specific contrast agent.

A, Representative short-axis images of relaxation rate (R_1, left columns) maps and tropoelastin immunohistochemistry (IHC; right columns) of the hearts sections at 7, 14, and 21 days post-myocardial infarction (MI) at 3T magnetic resonance imaging (MRI). Tropoelastin fibers were identified as black fine fiber network. **B**, Quantification of the R_1 in the infarct, remote myocardium (N=8/time-point) and in SHAM-operated animals (N=6 per time-point). R_1 values increased significantly from 7 to 21 days post-MI. **C**, IHC quantification, showing a significant increase in tropoelastin fibers from 7 to 21 days post-MI (N=4/time-point; N=3 SHAM; $P_{Kruskal\text{-}Wallis}$ SHAM vs 21 days <0.01). **D**, Correlation between ex vivo measurements of tropoelastin IHC and in vivo R_1 values of the scar. Spearman correlation (N=16, ρ=0.89, *P*<0.0001). Scale bar, 50 µm. **P*<0.05, ***P*<0.01, ****P*<0.001.

operating characteristic analysis (Figure IV in the Data Supplement). Both measurements carry some predictive value (R_1<2.34: [Sens(%)+IC95%]=54.5 [22.0–87.0]; [Specif(%)+IC95%]=100 [92.1–100.0]; 0.55<^{19}F<1.85: [Sens(%)+IC95%]=50 [20.5–79.5]; [Specif(%)+IC95%]=82 [59.3–100.0]) but the combination of both improved the sensitivity and specificity in identifying animals that underwent

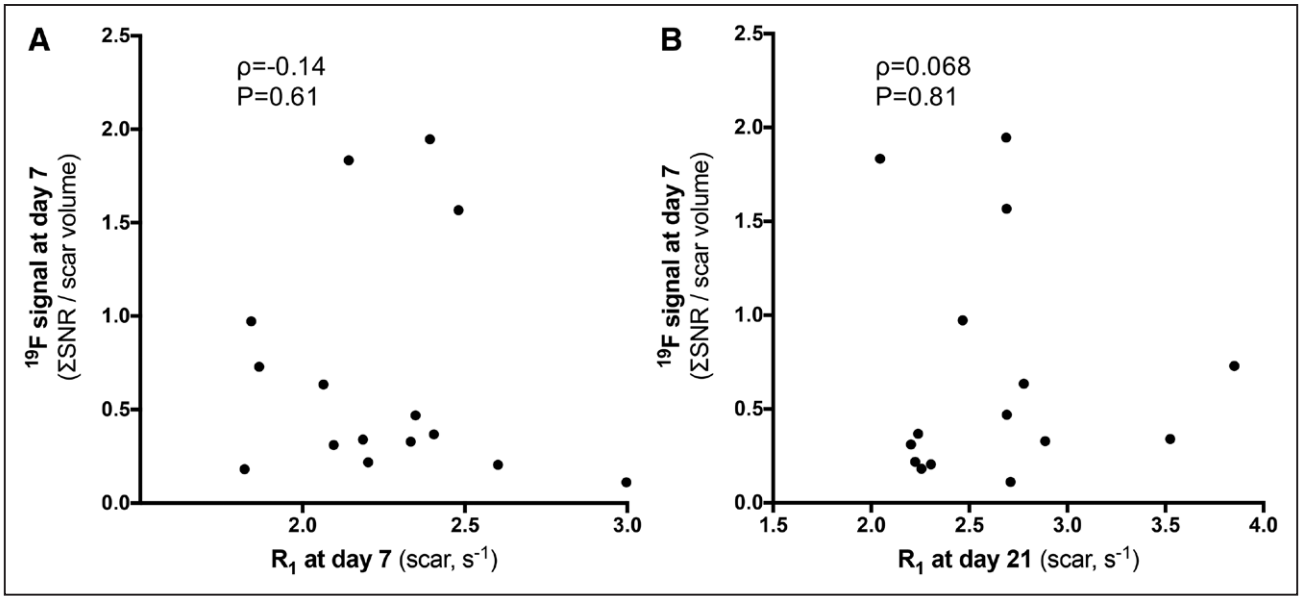

Figure 6. Correlation between ^{19}F signal and Gd-ESMA.
There is no correlation between ^{19}F signal at day 7 and (**A**) Gd-ESMA uptake 7 days after myocardial infarction (MI) and (**B**) gadolinium-based elastin/tropoelastin specific MR contrast agent (Gd-ESMA) uptake in the infarcted myocardium at day 21 post-MI.

favorable myocardial remodeling post-MI (R_1<2.34 and 0.55<^{19}F<1.85: [Sens(%)+IC95%]=75 [49.4–100.0], [Specif(%)+IC95%]=91 [74.1–100.0]). Logistic regression analysis using the increase of EDV at day 21 (dysfunctional remodeling) or the decrease of EDV at day 21 (beneficial remodeling) as outcome result, showed that R_1 at day 7 and ^{19}F at day 7 were not significant predictors by themselves (*P*=0.68 and *P*=0.062, respectively). However, the combination of both measurement results in an odds ratio of 30.0 (CI 95%, 1.41–638.15; *P*=0.029).

DISCUSSION

In this cross-sectional study we showed that (1) PFCs ^{19}F MRI can be used to assess and monitor inflammatory cell recruitment in vivo in the injured myocardium at a clinical field strength, as confirmed by ex vivo NMR and histological studies; (2) Gd-ESMA MRI allows quantification and visualization of scar size and elastin/tropoelastin deposition in the myocardium during the scar maturation phase; and (3) in a longitudinal proof-of-concept study, we further investigated the merits of

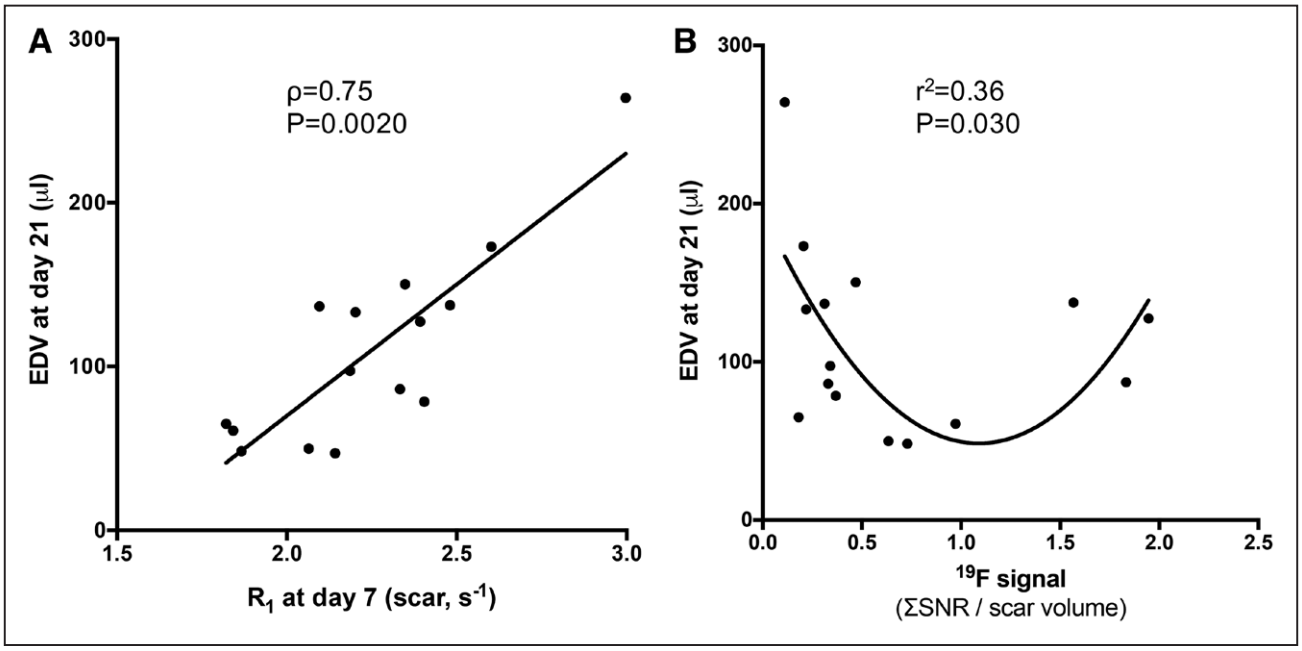

Figure 7. Correlation between end-diastolic volume (EDV) at day 21 and R1 values and ^{19}F signal at day 7.
A, Linear correlation was found between EDV and R_1 (gadolinium-based elastin/tropoelastin specific MR contrast agent [Gd-ESMA] uptake). **B**, Quadratic regression was found between EDV and ^{19}F signal-to-noise ratio (SNR).

both biomarkers for the prediction of the amount of cardiac remodeling (measured as EDV). We found that at the early stages post-MI a weak or strong inflammatory response results in dysfunctional MI healing and that increased elastin/tropoelastin deposition within the scar tissue at the 7 day's time-point is detrimental for cardiac remodeling. Our results suggest that multinuclear $^{19}F/^{1}H$ MRI may provide a better understanding of the biological processes underlying post-MI remodeling in vivo and PFCs and Gd-ESMA may serve as new imaging biomarkers for monitoring the progression of cardiac disease and allow predicting outcome.

Within the first week after MI inflammatory cells are recruited to the site of injury. Phagocytes avidly take up PFCs, which can be imaged by ^{19}F MRI with excellent contrast and without unwanted background signal, as shown previously.[11,14,22,23] However, no study has described the temporal evolution of ^{19}F signal in vivo at clinical field strength. Here we investigated the time course of inflammation using PFCs in vivo in a model of MI and related with the presence of immune cells. We successfully demonstrated the noninvasive visualization and quantification of inflammatory cells with PFCs in the infarcted region in a murine model of MI by in vivo MRI, validated ex vivo by NMR. MRI signal intensity measurements demonstrated that ^{19}F is detectable within the first-week post-MI, with a peak at 7 days, and importantly, PFC accumulation was restricted only to the infarcted region. Consistent with these findings, histological analysis showed that monocyte/macrophage populations are significantly increased up to 7 days after LAD occlusion as detected by immune positive MAC-3 staining and, furthermore, we found a strong correlation between MAC-3 and ^{19}F MRI signal. Our results are also in good agreement with the resolution of inflammatory response at days 14 and 21 as described in animal models of MI.[2,24,25]

Noninvasive imaging of inflammatory cells recruitment to the injured and remote myocardium has been shown by positron emission tomography in vivo[26] but requires special patient preparation to suppress myocardial glucose metabolism. Alternatively, magnetic nanoparticles have been used for macrophage imaging post-MI in vivo[27]; however, despite their excellent sensitivity, they generate negative contrast because of shortened T_2/T_2^* relaxation times of nearby water protons, creating hypointense regions and consequently making quantification challenging. Moreover, magnetic nanoparticles cannot be used in combination with other Gd-based contrast agents. In contrast, PFCs are detected directly and, therefore, generate positive signal contrast, and more importantly can be imaged simultaneously with, for example, Gd-based contrast agents affecting only the extracellular ^{1}H signal while ^{19}F PFCs will be located intracellularly after phagocytosis. The potential of ^{19}F particles has been extensively explored in preclinical models; they are chemically stable and can be further functionalized by adding fluorochromes, thus allowing multimodal imaging (eg, MRI and fluorescence imaging). In this work, we did not investigate if PFCs can differentiate between the monocyte/macrophage subpopulations ($Ly6C^{high}$ versus $Ly6C^{low}$; M1 versus M2) during post-MI remodeling in vivo, which would be of great interest. Previous publications have suggested the recruitment of macrophages to the remote myocardium[26,27]; here, because of sensitivity we could not detect myocardial leukocyte enrichment. Nevertheless, ^{19}F MRI may provide an in vivo readout for monitoring treatment-related changes in total inflammatory cell infiltration.

As the inflammatory process dissipates, fibrotic tissue accumulates in the infarcted regions and is then replaced by ECM proteins. Scar tissue formation commences as early as 1-week post-MI and is mainly composed of collagen type I but also elastin. Elastin is an insoluble protein that has been associated with scar formation and stabilization.[8,28,29] Mature elastin is formed by cross-linking of its soluble precursor, tropoelastin. Here, we took advantage of the increasing expression of elastin/tropoelastin during post-MI remodeling and investigated the use of Gd-ESMA as an imaging biomarker for the assessment of ECM remodeling. Elastin/tropoelastin was quantified using T_1 mapping to measure R_1 after Gd-ESMA injection with 3T MRI. R_1 values significantly increased from 7 to 21 days post-MI, which was in good agreement with the deposition of tropoelastin in the infarcted area measured by histology. At 3 days post-MI, T_1 mapping showed a significant increase in R_1 in the infarcted area, however, histology showed a lack of elastin/tropoelastin at this time point. We hypothesized that Gd-ESMA acts similarly to other gadolinium-based contrast agents because of its small size,[17,30] and immediately after MI its retention within the infarcted region may be unspecific and attributed to edema, cellular swelling and rupture, and subsequent increase in extracellular volume, as previously shown in dogs and humans.[19–21] Consistent with this hypothesis, we observed a high-signal intensity on native T2-weighted images at day 3 (high water content) in the infarcted area, which decreased at day 7 post-MI. Additionally, Gd-ESMA not only binds to tropoelastin and elastin (41%, K_D=9.2±0.7 μM; 40%, K_D=1.0±0.5 μM, respectively) but also to other proteins, including BSA (15%, K_D=ns) and chondroitin sulfates (5%, K_D=ns),[31,32] collagen types I and III (22%, K_D=7.3±1.3 μM; 13%, K_D=6.8±1.2 μM, respectively)[18] that might be present at day 3, thus increasing its retention and tissue relaxation.

Gd-ESMA has been successfully used for molecular imaging of vessel wall elastin in atherosclerosis (30–32), and myocardial scar.[15] ECM remodeling could also be assessed with alternative contrast agents specific for

other matrix proteins such as collagen thereby providing additional biological information in addition to standard LGE-MRI.

The recovery of cardiac function after MI is highly dependent on a balanced inflammatory response and on the deposition of ECM proteins within the heart. In our longitudinal proof-of-principle study the impact of the inflammatory response on LV remodeling was evaluated with PFCs and ECM remodeling with Gd-ESMA MRI. A moderate inflammatory response at day 3 (intermediate ^{19}F signal) was associated with a better LV remodeling at day 21 (measured as EDV). The healing process is affected by the exposure and duration of acute inflammation. Prolonged and exacerbated inflammation has been related to worse prognosis and similarly, the lack of inflammation has been associated with thinner infarcts, where the myocardium is more likely to rupture.[3,4] A certain degree of inflammation and a controlled recruitment of monocyte/macrophages populations seems to be desired for optimal MI healing. Likewise, Sahul et al[33] have shown that moderate amounts of metalloproteinases in the infarcted region lead to lower LV remodeling in a pig model of MI. Inflammatory cell migration toward the infarct requires the presence of metalloproteinases to facilitate migration. Interestingly, while metalloproteinases are crucial for the recruitment of inflammatory cells, this study has shown that excessive metalloproteinases activation leads to LV expansion.

Here, we also have shown that higher R_1 values at 7 days (high elastin/tropoelastin deposition) were associated with an unfavorable prognosis at 21 days post-MI (high EDV). In previous work, Gd-ESMA has also been used to assess elastin deposition in the heart in a mouse model of MI. In their cross-sectional study, Wildgruber et al[17] found that a higher contrast to noise ratio between scar and remote myocardium at day 21 correlated with a higher ejection fraction at the same time point, whereas the contrast to noise ratio at day 7 did not predict outcome at day 21. In contrast, we performed a longitudinal study, using T_1 mapping and EDV as a readout for LV remodeling. Other studies showed that modifying the composition of myocardial scar by exogenously increasing elastin content, cardiac function was improved after MI in rats.[7–9] Also, increased expression of elastin via cell-based gene therapy improved cardiac function and survival of ischemic hearts in a rat model of MI.[8,34] Further studies are needed to pinpoint the long-term role of elastin turnover/metabolism and cross-linking after MI.

Finally, we have also shown that the combination of the R_1 at day 7 and ^{19}F at day 7 could predict the beneficial or dysfunctional LV remodeling, although the odds ratio is statistically significant, it has a wide CI, which reflex the complex process of inflammation and remodeling, further studies, including bigger sample size and different animal models, have to be used to validate this conclusion.

Overall, multinuclear ^{19}F/^{1}H MRI may improve our knowledge of cardiac remodeling in vivo by targeting key biological processes that are responsible for post-MI remodeling. This imaging protocol may be useful for risk stratification or to facilitate the in vivo study of the effects of novel therapeutic procedures in disease progression and potentially personalization of therapy.

LIMITATIONS

This study has shown the feasibility of multinuclear imaging in a murine model of post-MI remodeling via LAD ligation. ^{19}F imaging was performed in a small-animal model using a clinical 3T MR scanner, where high amounts of PFCs (ie, 3 mmol PFC per kilogram body weight) are required to generate enough signal. The high-dosage enabled visualization of PFCs in small structures such as the murine heart. For early time-points ^{19}F deposition colocalized with LGE-ESMA enhancement within the scar area; however, for days 14 and 21 LGE-ESMA images were used as guide for the analysis of PFC uptake. Direct quantification of PFCs from the MRI could not be performed, as a surface coil was used. However, with the use of NMR experiments at 9.4T we were able to quantify PFCs content both in the remote and infarcted myocardium ex vivo. As PFCs used in this study were not specific for macrophages, signal accumulation in the infarct area might also be because of other cells with phagocytic capacity. PFC accumulation is not specific for myocardial inflammation but can also occur at other sites of inflammation (thoracotomy) and organs with high amounts of inflammatory and phagocytic cells such as the liver and lymph nodes. The here used PFCs did not allow to differentiate between the monocyte/macrophage subpopulations (Ly6C^{high} versus Ly6C^{low}; M1 versus M2) during post-MI remodeling in vivo. PFC injection did not show any adverse effects in the animals throughout the period of time animals were monitored. However, PFCs have long-retention time in the body, making it challenging to obtain approval for clinical application. Further, improvement of the PFC nanoparticles biodistribution properties, while maintaining their specificity for macrophages could aid future use in humans. Additionally, in our study, we used a higher the dose of Gd-ESMA (0.5 mmol/kg) compared with that used in other animal models (0.2 mmol/kg) or nontargeted gadolinium-based agents in clinical studies. Future experiments will require dose optimization in MI models or humans; however, no toxic effects have been observed in the animals at any time-point. Finally, we used a permanent LAD occlusion model demonstrating a strong acute inflammatory response for proof-of-concept ^{19}F/^{1}H MRI of myocardial inflammation

and remodeling after MI. In future studies, a reperfusion model will be investigated, as it is more clinically relevant. The permanent LAD occlusion model only produces a mild inflammatory response, whereas the reperfusion model typically results in a stronger inflammatory response. Although the inflammatory response was weaker in our model we were able to detect and quantify both inflammation and ECM deposition in the infarct zone, making these contrast agents promising biomarkers for future studies.

CONCLUSIONS

We successfully demonstrated the feasibility of multinuclear $^{1}H/^{19}F$ MRI to noninvasively assess and quantify the inflammatory response and evaluate elastin formation after post-MI remodeling in a murine model in vivo. We further studied the interplay between these biological processes and correlated those with LV remodeling. This novel approach has potential for monitoring treatment effects that aim to modulate the inflammatory or elastin responses in vivo and may aid the prognosis of cardiovascular diseases.

ARTICLE INFORMATION

Received December 12, 2017; accepted August 4, 2018.

The Data Supplement is available at https://www.ahajournals.org/doi/suppl/10.1161/CIRCIMAGING.117.007453.

Correspondence

Isabel T. Ramos, PhD, School of Biomedical Engineering and Imaging Sciences, The Rayne Institute, 4th Floor, Lambeth Wing, St. Thomas' Hospital, London, SE1 7EH, United Kingdom. Email isabel.ramos@kcl.ac.uk

Affiliations

School of Biomedical Engineering and Imaging Sciences, King's College London, United Kingdom (I.T.R., M.H., M.N., B.L., S.L., P.G., A.P., T.R.E., A.P., R.M.B.). School of Cardiovascular Medicine and Sciences, King's College London British Heart Foundation Centre of Excellence, United Kingdom (I.T.R., B.L., S.L., A.P., A.M.S.). Department of Physics of Molecular Imaging Systems, Institute for Experimental Molecular Imaging, RWTH Aachen University, Germany (P.G.). Radiology Department, School of Medicine (M.E.A.) and Escuela de Ingeniería (R.M.B.), Pontificia Universidad Catolica de Chile, Santiago. Department of Molecular Cardiology, Heinrich Heine University Duesseldorf, Germany (U.F.).

Sources of Funding

This work was supported by a King's College London British Heart Foundation Centre of Excellence inter-disciplinary PhD fellowship, a British Heart Foundation Program grant (RG/12/1/29262) and the Wellcome Trust/Engineering and Physical Sciences Research Council (EPSRC) Centre for Medical Engineering (NS/A000049/1 and WT 203148/Z/16/Z).

Disclosures

None.

REFERENCES

1. Frangogiannis NG. The inflammatory response in myocardial injury, repair, and remodelling. *Nat Rev Cardiol*. 2014;11:255–265. doi: 10.1038/nrcardio.2014.28
2. Frangogiannis NG. Regulation of the inflammatory response in cardiac repair. *Circ Res*. 2012;110:159–173. doi: 10.1161/CIRCRESAHA.111.243162
3. Pfeffer MA, Braunwald E. Ventricular remodeling after myocardial infarction. Experimental observations and clinical implications. *Circulation*. 1990;81:1161–1172.
4. Solomon SD, Glynn RJ, Greaves S, Ajani U, Rouleau JL, Menapace F, Arnold JM, Hennekens C, Pfeffer MA. Recovery of ventricular function after myocardial infarction in the reperfusion era: the healing and early afterload reducing therapy study. *Ann Intern Med*. 2001;134:451–458. doi: 10.7326/0003-4819-134-6-200103200-00009
5. Bassett EG, Wakefield JS. Elastic fibers in myocardial scars in rats: development teraction with other components. *Connect Tissue Res*. 2008;49:321–327. doi: 10.1080/03008200801913270
6. Whittaker P, Boughner DR, Kloner RA. Role of collagen in acute myocardial infarct expansion. *Circulation*. 1991;84:2123–2134.
7. Mizuno T, Mickle DA, Kiani CG, Li RK. Overexpression of elastin fragments in infarcted myocardium attenuates scar expansion and heart dysfunction. *Am J Physiol Heart Circ Physiol*. 2005;288:H2819–H2827. doi: 10.1152/ajpheart.00862.2004
8. Mizuno T, Yau TM, Weisel RD, Kiani CG, Li RK. Elastin stabilizes an infarct and preserves ventricular function. *Circulation*. 2005;112(suppl 9):I81–I88. doi: 10.1161/01.CIRCULATIONAHA.105.523795
9. Lichtenauer M, Mildner M, Baumgartner A, Hasun M, Werba G, Beer L, Altmann P, Roth G, Gyöngyösi M, Podesser BK, Ankersmit HJ. Intravenous and intramyocardial injection of apoptotic white blood cell suspensions prevents ventricular remodelling by increasing elastin expression in cardiac scar tissue after myocardial infarction. *Basic Res Cardiol*. 2011;106:645–655. doi: 10.1007/s00395-011-0173-0
10. Ramos IT, Henningsson M, Nezafat M, Lavin B, Lorrio S, Gebhardt P, Protti A, Eykyn TR, Andia ME, Flogel U, Phinikaridou A, Shah AM, Botnar RM. Simultaneous Assessment of Cardiac Inflammation and Extracellular Matrix Remodeling After Myocardial Infarction. *figshare*. DOI: 10.6084/m9.figshare.5968963 (2018).
11. Flögel U, Ding Z, Hardung H, Jander S, Reichmann G, Jacoby C, Schubert R, Schrader J. In vivo monitoring of inflammation after cardiac and cerebral ischemia by fluorine magnetic resonance imaging. *Circulation*. 2008;118:140–148. doi: 10.1161/CIRCULATIONAHA.107.737890
12. Nezafat M, Ramos IT, Henningsson M, Protti A, Basha T, Botnar RM. Improved segmented modified Look-Locker inversion recovery T1 mapping sequence in mice. *PLoS One*. 2017;12:e0187621. doi: 10.1371/journal.pone.0187621
13. Protti A, Sirker A, Shah AM, Botnar R. Late gadolinium enhancement of acute myocardial infarction in mice at 7T: cine-FLASH versus inversion recovery. *J Magn Reson Imaging*. 2010;32:878–886. doi: 10.1002/jmri.22325
14. Ebner B, Behm P, Jacoby C, Burghoff S, French BA, Schrader J, Flögel U. Early assessment of pulmonary inflammation by 19F MRI in vivo. *Circ Cardiovasc Imaging*. 2010;3:202–210. doi: 10.1161/CIRCIMAGING.109.902312
15. Protti A, Lavin B, Dong X, Lorrio S, Robinson S, Onthank D, Shah AM, Botnar RM. Assessment of myocardial remodeling using an elastin/tropoelastin specific agent with high field magnetic resonance imaging (MRI). *J Am Heart Assoc*. 2015;4:e001851. doi: 10.1161/JAHA.115.001851
16. Jacoby C, Temme S, Mayenfels F, Benoit N, Krafft MP, Schubert R, Schrader J, Flögel U. Probing different perfluorocarbons for in vivo inflammation imaging by 19F MRI: image reconstruction, biological half-lives and sensitivity. *NMR Biomed*. 2014;27:261–271. doi: 10.1002/nbm.3059
17. Wildgruber M, Bielicki I, Aichler M, Kosanke K, Feuchtinger A, Settles M, Onthank DC, Cesati RR, Robinson SP, Huber AM, Rummeny EJ, Walch AK, Botnar RM. Assessment of myocardial infarction and postinfarction scar remodeling with an elastin-specific magnetic resonance agent. *Circ Cardiovasc Imaging*. 2014;7:321–329. doi: 10.1161/CIRCIMAGING.113.001270
18. Botnar RM, Wiethoff AJ, Ebersberger U, Lacerda S, Blume U, Warley A, Jansen CH, Onthank DC, Cesati RR, Razavi R, Marber MS, Hamm B, Schaeffter T, Robinson SP, Makowski MR. In vivo assessment of aortic aneurysm wall integrity using elastin-specific molecular magnetic resonance imaging. *Circ Cardiovasc Imaging*. 2014;7:679–689. doi: 10.1161/CIRCIMAGING.113.001131
19. Abdel-Aty H, Cocker M, Meek C, Tyberg JV, Friedrich MG. Edema as a very early marker for acute myocardial ischemia: a cardiovascular magnetic resonance study. *J Am Coll Cardiol*. 2009;53:1194–1201. doi: 10.1016/j.jacc.2008.10.065
20. Dall'Armellina E, Karia N, Lindsay AC, Karamitsos TD, Ferreira V, Robson MD, Kellman P, Francis JM, Forfar C, Prendergast BD, Banning AP, Channon KM, Kharbanda RK, Neubauer S, Choudhury RP. Dynamic changes of edema and late gadolinium enhancement after acute myocardial infarction and their relationship to functional recovery and salvage index. *Circ Cardiovasc Imaging*. 2011;4:228–236. doi: 10.1161/CIRCIMAGING.111.963421

21. Willerson JT, Scales F, Mukherjee A, Platt M, Templeton GH, Fink GS, Buja LM. Abnormal myocardial fluid retention as an early manifestation of ischemic injury. *Am J Pathol*. 1977;87:159–188.
22. Flögel U, Su S, Kreideweiss I, Ding Z, Galbarz L, Fu J, Jacoby C, Witzke O, Schrader J. Noninvasive detection of graft rejection by in vivo (19) F MRI in the early stage. *Am J Transplant*. 2011;11:235–244. doi: 10.1111/j.1600-6143.2010.03372.x
23. Temme S, Bönner F, Schrader J, Flögel U. 19F magnetic resonance imaging of endogenous macrophages in inflammation. *Wiley Interdiscip Rev Nanomed Nanobiotechnol*. 2012;4:329–343. doi: 10.1002/wnan.1163
24. Frangogiannis NG. Targeting the inflammatory response in healing myocardial infarcts. *Curr Med Chem*. 2006;13:1877–1893. doi: 10.2174/092986706777585086
25. Jaffer FA, Sosnovik DE, Nahrendorf M, Weissleder R. Molecular imaging of myocardial infarction. *J Mol Cell Cardiol*. 2006;41:921–933. doi: 10.1016/j.yjmcc.2006.09.008
26. Lee WW, Marinelli B, van der Laan AM, Sena BF, Gorbatov R, Leuschner F, Dutta P, Iwamoto Y, Ueno T, Begieneman MP, Niessen HW, Piek JJ, Vinegoni C, Pittet MJ, Swirski FK, Tawakol A, Di Carli M, Weissleder R, Nahrendorf M. PET/MRI of inflammation in myocardial infarction. *J Am Coll Cardiol*. 2012;59:153–163. doi: 10.1016/j.jacc.2011.08.066
27. Alam SR, Shah AS, Richards J, Lang NN, Barnes G, Joshi N, MacGillivray T, McKillop G, Mirsadraee S, Payne J, Fox KA, Henriksen P, Newby DE, Semple SI. Ultrasmall superparamagnetic particles of iron oxide in patients with acute myocardial infarction: early clinical experience. *Circ Cardiovasc Imaging*. 2012;5:559–565. doi: 10.1161/CIRCIMAGING.112.974907
28. Yanagisawa H, Davis EC, Starcher BC, Ouchi T, Yanagisawa M, Richardson JA, Olson EN. Fibulin-5 is an elastin-binding protein essential for elastic fibre development in vivo. *Nature*. 2002;415:168–171. doi: 10.1038/415168a
29. Kielty CM, Sherratt MJ, Shuttleworth CA. Elastic fibres. *J Cell Sci*. 2002;115(pt 14):2817–2828.
30. Makowski MR, Wiethoff AJ, Blume U, Cuello F, Warley A, Jansen CH, Nagel E, Razavi R, Onthank DC, Cesati RR, Marber MS, Schaeffter T, Smith A, Robinson SP, Botnar RM. Assessment of atherosclerotic plaque burden with an elastin-specific magnetic resonance contrast agent. *Nat Med*. 2011;17:383–388. doi: 10.1038/nm.2310
31. von Bary C, Makowski M, Preissel A, Keithahn A, Warley A, Spuentrup E, Buecker A, Lazewatsky J, Cesati R, Onthank D, Schickl N, Schachoff S, Hausleiter J, Schömig A, Schwaiger M, Robinson S, Botnar R. MRI of coronary wall remodeling in a swine model of coronary injury using an elastin-binding contrast agent. *Circ Cardiovasc Imaging*. 2011;4:147–155. doi: 10.1161/CIRCIMAGING.109.895607
32. Phinikaridou A, Andia ME, Indermuehle A, Onthank DC, Cesati RR, Smith A, Robinson SP, Saha P, Botnar RM. Vascular remodeling and plaque vulnerability in a rabbit model of atherosclerosis: comparison of delayed-enhancement MR imaging with an elastin-specific contrast agent and unenhanced black-blood MR imaging. *Radiology*. 2014;271:390–399. doi: 10.1148/radiol.13130502
33. Sahul ZH, Mukherjee R, Song J, McAteer J, Stroud RE, Dione DP, Staib L, Papademetris X, Dobrucki LW, Duncan JS, Spinale FG, Sinusas AJ. Targeted imaging of the spatial and temporal variation of matrix metalloproteinase activity in a porcine model of postinfarct remodeling: relationship to myocardial dysfunction. *Circ Cardiovasc Imaging*. 2011;4:381–391. doi: 10.1161/CIRCIMAGING.110.961854
34. Li SH, Sun Z, Guo L, Han M, Wood MF, Ghosh N, Vitkin IA, Weisel RD, Li RK. Elastin overexpression by cell-based gene therapy preserves matrix and prevents cardiac dilation. *J Cell Mol Med*. 2012;16:2429–2439. doi: 10.1111/j.1582-4934.2012.01560.x